This work was carried out in whole or in part within the framework of the NOMATEN Center of Excellence, supported from the European Union Horizon 2020 research and innovation programme (Grant Agreement No. 857470) and from the European Regional Development Fund via the Foundation for Polish Science International Research Agenda PLUS programme (Grant No. MAB PLUS/2018/8).

This is the accepted manuscript submitted to: International Journal of Refractory Metals and Hard Materials, vol 105, June 2022, 105811, published on 24 February 2022 with the embargo period till: 24 February 2024.

DOI: 10.1016/j.ijrmhm.2022.105811

Thermal and mechanical properties of (W,Zr)B_{2-z} coatings deposited by RF magnetron sputtering method

Tomasz Mościcki[1], Justyna Chrzanowska-Giżyńska[1*], Rafał Psiuk[1], Piotr Denis[1], Katarzyna Mulewska[2] Łukasz Kurpaska[2], Marcin Chmielewski[3], Maria Wiśniewska[4], Dariusz Garbiec[4]

[1]Institute of Fundamental Technological Research, Polish Academy of Sciences, Pawińskiego 5B, 02-106 Warsaw, Poland

[2]National Centre for Nuclear Research, A. Soltana 4, 05-400 Otwock, Poland

[3]Łukasiewicz Research Network Institute of Electronic Materials Technology, Wółczyńska 133, 01-919 Warsaw, Poland

[4]Metal Forming Institute, Jana Pawła II 14, 61-139 Poznań, Poland

*corresponding author: jchrzan@ippt.pan.pl

Abstract:

Magnetron sputtered WB_2 coatings doped with 8, 11 and 16 at.% zirconium were analysed using energy dispersive spectroscopy, X-ray diffraction and nanoindentation under the load of 4, 7 and 10 mN. It has been observed that these coatings crystallize in the α-AlB_2 and ω-W_2B_5 prototype structure. Phenomenon responsible for this is an increase of the zirconium content which causes an increase in the ω-W_2B_5 phase. All the deposited coatings have a hardness of about 45 Gpa, while Young's modulus drops down from 497 to 480 GPa with increasing Zr content. Coatings without doping and doped with 16 at.% zirconium were annealed at 650°C and subjected to cyclic thermal loads using a maximum temperature 600°C and cooling with a compressed air. It has been observed that addition of zirconium improved coatings phase stability.

1. Introduction

Tungsten borides are distinguished by their high hardness, high melting point, chemical, and thermal stability. This unique combination of properties results in application Ti_xB_y in the production of high-speed tools, dies (rod drawing), and brake discs. In recent years different tungsten borides compositions were tested [?]. However, the recent research is focused on a tungsten diboride because the results of numerical simulations as well as the experimental data indicate the hardness of this material to be over 40 GPa [1] while maintaining its perfect thermal stability up to 700°C [2]. Due to the possibility of microstructure formation, reported coatings exhibit even better properties in comparison with solid materials [3]. Moreover, WB_2 properties can be enhanced by the addition of Zr [4], Ti [5], Ta [6, 7], and N [**Błąd! Nie można odnaleźć źródła odwołania.**]. This effect is related to the improvement of the transformation temperature of the AlB_2-type WB_2 phase.

In this work we decided to focus on the effect of Zr doping on the properties of WB_2 coatings deposited in the magnetron sputtering process. The results of experimental research obtained to date show the formation of the non-equilibrium α-WB_2 phase [1, 7] even though ω-W_2B_5 is more thermodynamically stable [**Błąd! Nie można odnaleźć źródła odwołania.**]. The process of physical vacuum deposition synthesis is responsible for this effect [?]. It is known that this method is known to favor the formation of the point defects such as vacancies which stabilize the non-equilibrium phase. Referring to the results of Moraes' et al. [7, 8], one can see that vacancies can be further stabilized by (Zr?) doping, which favors the formation of the phase with negative formation energy. In the case of ZrB_2, formation energy is -0.987 eV, so even lower than the formation energy of already investigated TaB_2 (-0.649 eV).

In this work our goal is to obtain coatings with a hardness comparable to that of α-WB_2 and with higher thermal stability. Reported results suggest that we were able to achieve this via Zr doping of the tungsten diboride.

2. Materials and methods

Process of magnetron sputtering

The sputtering targets with a diameter of 25.4 mm were produced by Spark Plasma Sputtering (SPS) process from boron (purity: 95%, average particle size APS: 1 µm, Sigma Aldrich), tungsten (purity: 99.9%, APS: 25 µm, Sigma Aldrich), and zirconium (purity: 99.8%, APS: 250-350 µm, Sigma Aldrich). Powders were mixed for 30 min using a Turbula® T2F shaker-mixer (WAB, Switzerland) in the compositions presented in Tab. 1. The obtained powder mixtures were SPSed in vacuum using an HP D 25/3 (FCT Systeme, Germany). The SPS process parameters are as follow: sintering temperature - 1800°C, heating rate - 400°C/min, holding time - 24 min and compacting pressure 50 MPa. Targets were composed of MoB_2-type WB_2 and WB_4-type WB_4. AlB_2-type ZrB_2 phase was observed in Zr-doped targets, see Fig. 1. Detailed information on SPS targets can be found in Ref. [4].

Afterwards, each target was mounted in the water-cooled 1-ich magnetron sputtering cathode (Kurt J. Lesker). The deposition process was performed in a vacuum chamber initially pumped to $2 \cdot 10^{-5}$ mbar and then filled with an argon gas up to the working pressure of $9 \cdot 10^{-3}$ mbar. The gas flow of argon was set to be 19 mL/min. Prior to each deposition, the target was sputtered for 5 min in order to ensure its clean surface and stable sputtering conditions. During all experiments, power supplied to the magnetron cathode was maintained at the level of 50 W. Films were deposited for 45 min on Si (100) (Institute of Electronic Materials Technology, Poland) and tungsten carbide G15 substrates (skąd) heated up to 540°C and positioned 40mm in front of the target. The deposited coatings were about 1 µm thick.

Tab. 1. Weight content of tungsten, zirconium and boron in W/B W/Zr/B powder mixtures

Material composition	Tungsten	Zirconium	Boron
$WB_{2.5}$	12.202	-	1.795
$W_{0.92}Zr_{0.08}B_{2.5}$	11.635	0.502	1.861
$W_{0.84}Zr_{0.16}B_{2.5}$	11.025	1.042	1.931
$W_{0.76}Zr_{0.24}B_{2.5}$	10.366	1.624	2.007

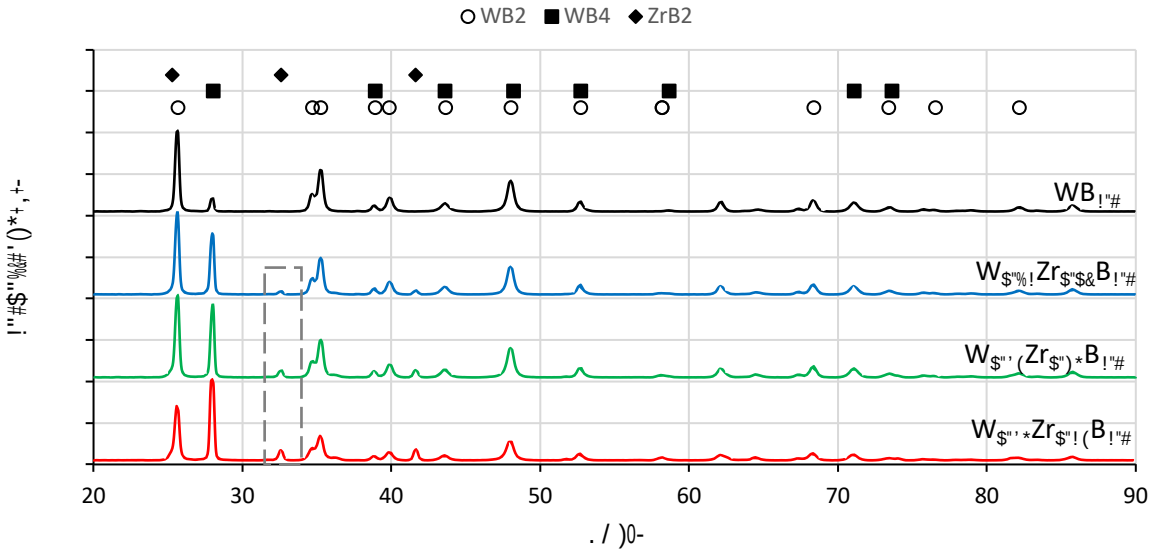

Fig. 1. XRD spectra of WB2.5 and $W_{1-x}Zr_xB_{2.5}$ SPS targets. Marked with dashed lines area shows growing intensity of the diffraction patterns, which indicates growing content of ZrB_2 phase.

Annealing and cycling temperature changes

Two types of coatings (WB_{2-x} and $W_{0.76}Zr_{0.16}B_{2-x}$) deposited on the tungsten carbide substrate were subjected to the heat treatment and the cyclic temperature changes.

Stability of both nanostructure and mechanical properties of the deposited coatings were studied after annealing at temperature of 650°C inside the vacuum chamber (PREVAC) pumped to a pressure of $2 \cdot 10^{-5}$ mbar. Samples were held at constant temperature for an hour and after the annealing, cooled down for 120 min to a temperature of 100 °C.

Described tests of cyclic temperature changes were carried out in the heating-cooling system ShockTherm (PESS Company), using a maximum temperature 600°C and cooling with a compressed air stream to room temperature. The temperature was controlled by thermocouples placed just above the samples. Individual heating-cooling cycle took approximately 180s, while the typical course of the process is presented in Fig. 2. Changes in the structure and evolution of layer properties were analysed after 10 and 50 heating-cooling cycles.

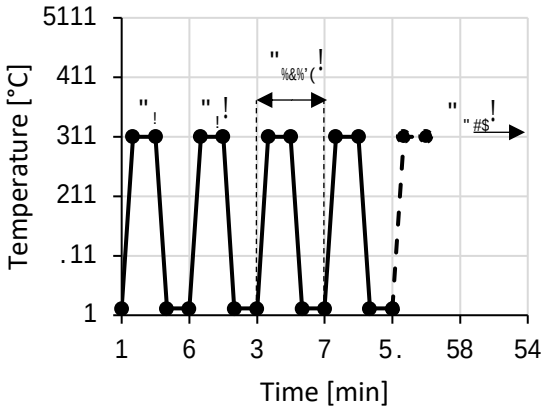

Fig. 2. Schematic view of the heating-cooling cycle.

Characterization

The surface microstructure and chemical composition were investigated using Scanning Electron

Microscope – SEM (JEOL JSM-6010Plus) equipped with Energy Dispersive X-Ray Spectroscope (EDS) detector. In 9:;$:(#9(<$#(#=$(>9%#(:$%*@?$(A*?,$%(9B(@9:9"(C9"#$"#0(the accelerating voltage was set to be 5 kV, according to Ref. [**Błąd! Nie można odnaleźć źródła odwołania.**]. Moreover, the system was calibrated with the use of commercially available target W_2B_5 (purity 99.9%, Huizhou Tian Yi Rare material Co. Ltd). It should be explained that the authors are aware of the uncertainties in boron measurement with EDS, which are related to the proximity of the boron and carbon peaks as well as carbon contamination. However, precise measurement of boron and tungsten at the same time is difficult with other techniques such as XPS as well. This is partially related to the accuracy of the calibration [**Błąd! Nie można odnaleźć źródła odwołania.**, **Błąd! Nie można odnaleźć źródła odwołania.**]. The crystal structure and phase composition of deposited layers were characterized by X-Ray Diffractometer (Bruker D8 Discover, λ=1.5418 Å) system. Measurements were taken in 2θ scan mode, with source fixed at 8° position. In this configuration, it was possible to avoid signal from the substrate while maintaining high intensity of the signal originating primarily from the studied coating.

Mechanical properties

Nanoindentation analyses were performed at room temperature using NanoTest Vantage (Micro Materials) system. Measurements were performed with Berkovich-shaped diamond indenter. The geometry of the indenter tip, so called Diamond Area Function, was calculated for each load and used when calculating mechanical parameters. Each indentation has been repeated 12 times and the measurements were made in the line with the distance of 50 um from each other. To minimize the effect of the substrate, the hardness and elastic modulus values were calculated based on the average data obtained at depths of about 100 nm (indentation load of 7 mN). The goal of this is to (i) ensure that the maximum indentation depth is not bigger than 1/10 of the coating thickness, thus minimizing substrate effect [**Błąd! Nie można odnaleźć źródła odwołania.**] and (ii) to measure hardness in load independent region, thus minimizing deformation created by the preceding indent [**Błąd! Nie można odnaleźć źródła odwołania.**].

3. Results and discussion

All the deposited coatings were smooth with a mean square roughness of 12±5 nm. No debris or delamination was observed, see Fig. 3a. Performed SEM-EDS analysis indicate that chemical elements composing $W_xZr_{1-x}B_{2-z}$ coatings after magnetron sputtered were homogeneously distributed in the whole volume of the coating (see Fig. 3b). The boron content B/(Zr+W) is in the range of 62.5- 74.6 at.% (1.36 - 1.59, see Fig. 4) which means that boron decreased by 36-46% compared to the target composition. A decrease of light elements has already been observed, e.g. in Ref. [3, **Błąd! Nie można odnaleźć źródła odwołania.**]. This phenomena may be related to the plasma scattering of light boron atoms (10.81 u) into heavy tungsten atoms (183.84 u). As a result of this, lower amount of boron seems to reach the substrate.

In the coatings deposited from zirconium-doped targets, the zirconium content dropped up to 34% in the comparison to initial target composition. The decrease in zirconium content, as in the case of boron, is predicted to be due to scattering of the zirconium atoms (91.224 u) on the tungsten atoms. Therefore, similar as previously described phenomena can be observed, resulting with lower Zr% then predicted.

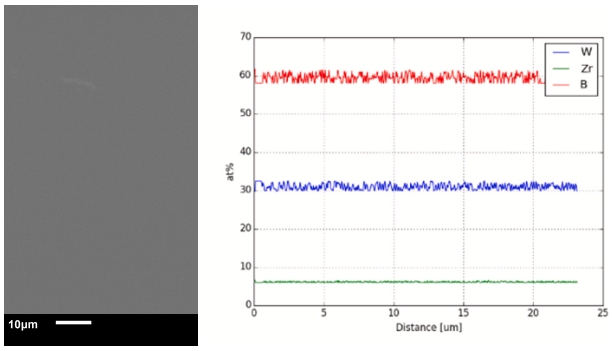

Fig. 3. a) SEM image of WB_{2-x}, b) EDS elemental maps of the coating deposited from the $W_{0.76}Zr_{0.24}B_{2-z}$ target

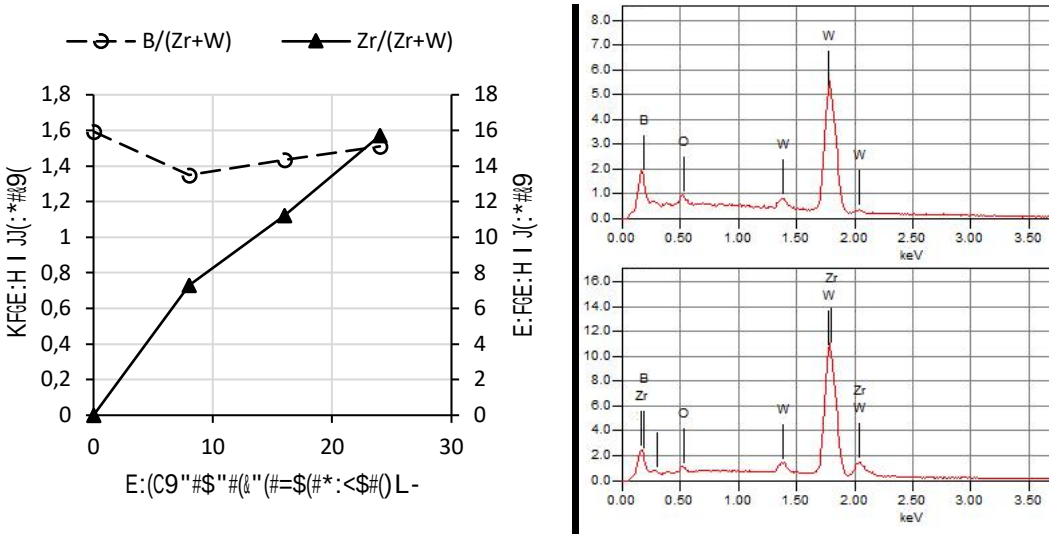

Fig. 4. Chemical composition of the deposited coatings a) B/(Zr+W) and Zr/(Zr+W) concentration, b) an example of EDS spectrum of the coating deposited from $WB_{2.5}$ (top) and $W_{0.76}Zr_{0.24}B_{2.5}$ target

The XRD spectrum of the deposited coatings revealed main diffraction peaks at 2θ ranging from about 24° to 31°, see Fig. 5a. In the case of WB_{2-z} coating, the peak positioned at 28.9° originates from the (001) plane of hexagonal AlB_2-type WB_2 (α-WB_2) while the peak positioned at 26° is derived from the (004) plane of hexagonal MoB_2-type WB_2 (ω-W_2B_5). Detailed deconvolution of XRD spectra leads to the determination of cell parameters as well as phase composition. The α-WB_2 phase has the following lattice parameters: a = 2.96 Å and c = 3.089 Å. At the same time the ω-W2B5 phase is characterized by the following lattice parameters: a = 3.076 Å, c = 13.684 Å. It should be explained that the theoretical parameters are as follows: a=3.020, c=3.050 [**Błąd! Nie można odnaleźć źródła odwołania.**] and a=2.983 Å, c=13.879 Å [**Błąd! Nie można odnaleźć źródła odwołania.**], respectively. The α-WB2 to ω-W2B5 ratio is 4.8 and both phases have similar crystallite size of 37 ± 2 nm (calculated on the basis of Scherrer formula). In the XRD spectrum, apart from narrow diffraction lines, a broad diffraction line at 2θ between 22° and 46° was observed. This data indicates the presence of the amorphous phase.

In the case of Zr-doped coatings the amorphous phase disappears, and the remaining diffraction lines (related to α-WB2 and ω-W_2B_5) are shifted towards smaller 2θ angles. Observed shift (toward smaller angles) increases with the increasing Zr content. The deconvolution of XRD spectra showed that experimentally obtained lattice parameters (both a and c) increase with increasing Zr content, see Fig. 6. Moreover, the α-WB_2 to ω-W_2B_5 ratio decreases with Zr, see Fig. 7. Reported

behaviour of doped WB_{2-z} coating has been already observed by Moraes et al.[7]. Moraes indicated that the shift in diffraction lines is related to boron vacancies in WB2 lattice and the formation of a new phase, in our case this is the W-Zr-B phase. Finally, obtained results point to the conclusion that the crystalline size of α-WB_2 and ω-W_2B_5 phases does not change significantly with increasing Zr content and is 30 and 40 nm, respectively.

The formation of non-equilibrium α and ω phases [**Błąd! Nie można odnaleźć źródła odwołania.**] has already been observed in Ref. [7, **Błąd! Nie można odnaleźć źródła odwołania.**]. As in the case of the coatings described in this work, studied by those two teams W-B coatings showed a boron deficiency in relation to the formed phases. Boron deficiency can be related to the coating deposition method. For example PVD methods are known to promote the incorporation of point defects such as vacancies during crystal growth. Moreover, it has been already shown in Ref. [7, **Błąd! Nie można odnaleźć źródła odwołania.**] that both the boron defects and the doping (contributing formation of the compound having very negative formation energy) increasing the ω phase stability. The formation energy of ZrB_2 is -0.987 eV. This is even lower than the formation energy of TaB_2 (-0.649 eV) which was analysed by Moraes et al. [7].

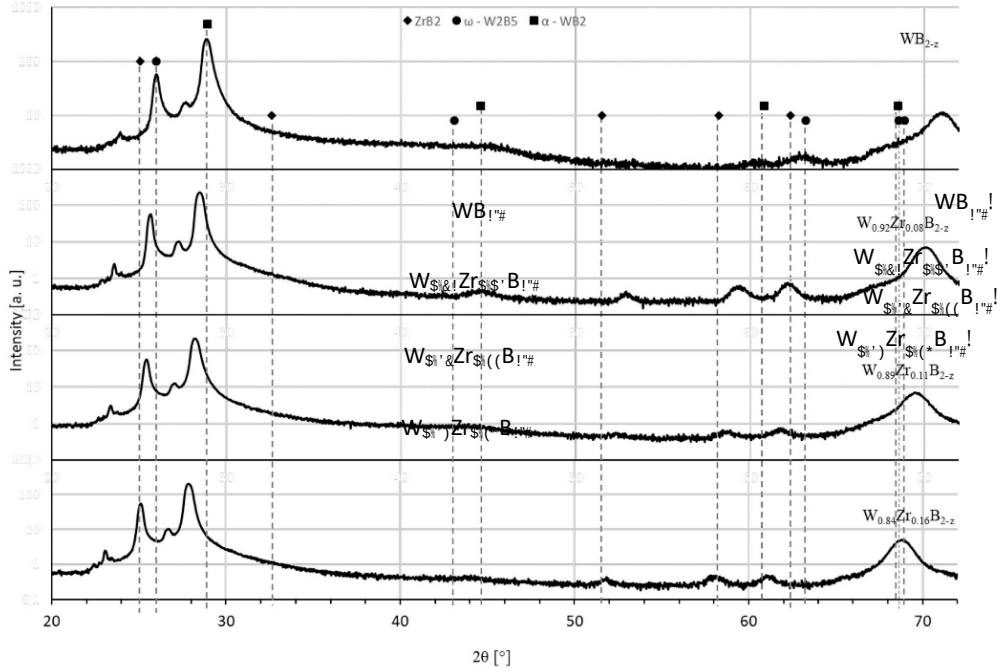

Fig. 5. Structural evolution of the as-deposited $W_{1-x}Zr_xB_{2-z}$ coatings with increasing Zr content (x = 0, 0.08, 0.11, 0.16). The standardized 2Θ-peak positions of ω – W_2B_5 (a=2.983 Å, c=13.879 Å) [!"#$%&'()&*+,-.&+$-./)01&023$".&+$4+".-(.5*, *α - WB_2 (a=3.020, c=3.050) [*!"#$%&'()&*+,-.&+$-./)01&023$".&+$4+".-(.5*] and AlB_2-type-ZrB_2 (a=3.170 Å , c=3.548 Å) are marked with circles, squares and filled rhombus symbols, respectively.*

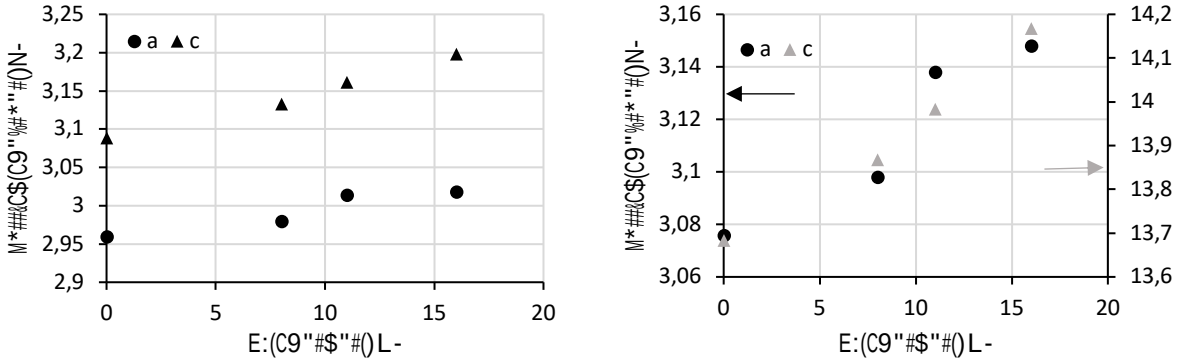

Fig. 6. The effect of Zr content on the lattice parameters a) α-WB_2, b) ω-W_2B_5. Triangle and circle stands for a and c lattice constant, respectively

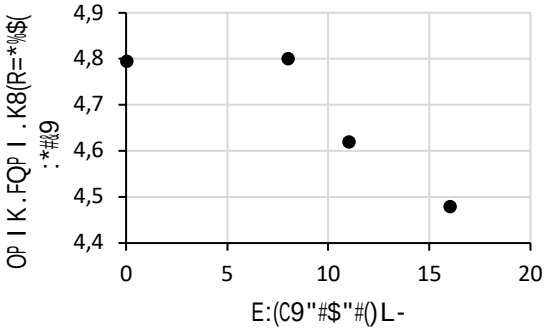

Fig. 7.The effect of Zr content on the phase composition of the deposited coating.

In the next step, detail nanomechanical investigation has been performed. The tests were made with loads of 4, 7 and 10 mN and the show that the plastic depth increases linearly with the load. The reported result indicates that conducted studies are made in a load-independent region, which suggest that developed plastic deformation under the indenter tip originates only from the coating, without the impact of the bulk material, see Fig. 8a. One can see that all the tested coatings, do not show an effect of pop-in on the loading region. Therefore, one can expect that up to the indentation load of 10 mN, crack initiation and propagation do not occur [**Błąd! Nie można odnaleźć źródła odwołania.**]. However, with an indentation load above 7 mN, small pop-out effect was observed. This is particularly visible for the WB_{2-x} system, see Fig. 8a,b. The observed phenomenon may be related to two phenomena: (i) the delamination of the coating from the substrate or (ii) temperature difference between indenter tip and the specimen. One should explain, that the samples were tested after 24h from the installation in the machine, i.e. any temperature differences should be removed by then. The pop-out free LD curves visible in the $W_{0.76}Zr_{0.16}B_{2-x}$ coating shows better adhesion of Zr-doped than pure WB_{2-x} coatings.

Mechanical properties of the coatings were compared for the indentation load of 7 mN. This was to avoid the maximum indentation depth exceeding 10% of the coating thickness. It was observed, that in the whole composition range, hardness of the deposited coatings did not change significantly (it varies from 44.5±1.6 to 46.2±1.6 GPa – line with rectangles). However, with increasing Zr content,

especially after reaching 10% level, the Young modulus drops down from 497±11 to 480±13 GPa, see Fig. 9.

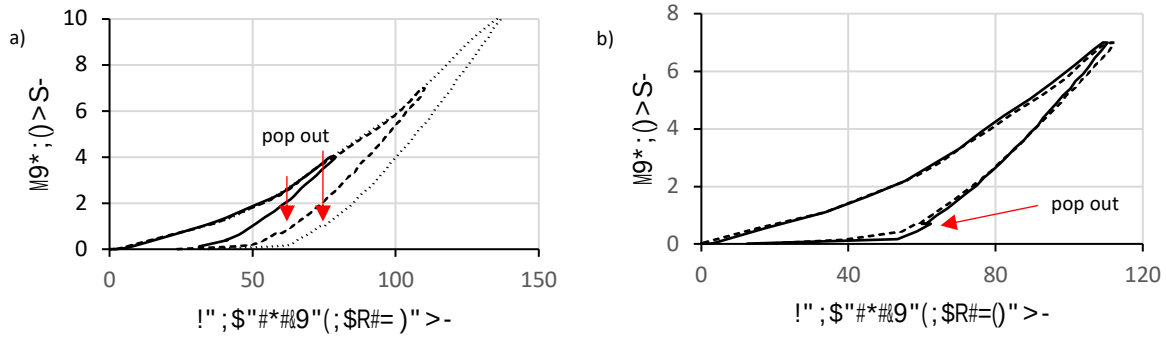

Fig. 8. Load-displacement curves of a) WB_{2-x} coating under maximum load of 5, 7 and 10 mN, b) WB_{2-x} (solid line) and $W_{0.76}Zr_{0.16}B_{2-x}$ (dotted line) under the maximum load of 7 mN. Pop-out effect can be observed in the WB_{2-x} unloading curves.

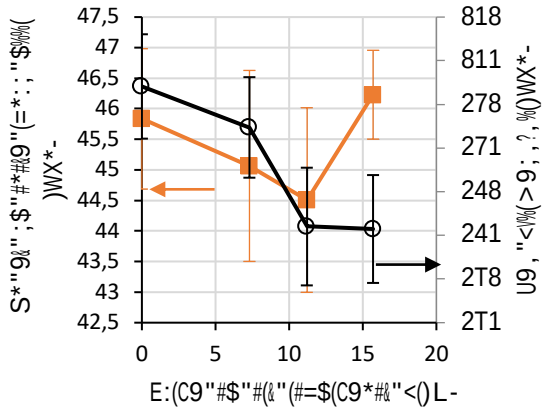

Fig. 9. Nanoindentation hardness and Young's modulus of WB_{2-z} coatings having different Zr content. Circles stands for Young's modulus, rectangles stands for hardness.

Table 2. Overview of the phases observed in the $W_{1-x}Zr_xB_{2-x}$ coatings.

Composition of the coating	Lattice constants of the as deposited coating	Phase composition of the coating after 1 h annealing	Phase composition after 50 shocks
WB_{2-z}	α-WB_2: a = 2.96 Å, c = 3.09 Å ω – W_2B_5: a = 3.08 Å, c = 13.68 Å	α-WB_2: a = 2.96 Å, c = 3.08 Å ω – W_2B_5: a = 3.08 Å, c = 13.78 Å	α-WB_2: a = 2.96 Å, c = 3.11 Å ω – W_2B_5: a = 3.08 Å, c = 13.78 Å
$W_{0.92}Zr_{0.08}B_{2-z}$	α-WB_2: a = 2.98 Å, c = 3.13 Å ω – W_2B_5: a = 3.11 Å, c = 13.87 Å	–	–
$W_{0.89}Zr_{0.11}B_{2-z}$	α-WB_2: a = 2.99 Å, c = 3.16 Å ω – W_2B_5: a = 3.14 Å, c = 13.98 Å	–	–
$W_{0.84}Zr_{0.16}B_{2-z}$	α-WB_2: a = 3.03 Å, c = 3.2 Å ω – W_2B_5: a = 3.17 Å, c = 14.17 Å	α-WB_2: a = 3.05 Å, c = 3.22 Å ω – W_2B_5: a = 3.20 Å, c = 14.21 Å	α-WB_2: a = 3.05 Å, c = 3.24 Å ω – W_2B_5: a = 3.21 Å, c = 14.21 Å
Theoretical α-WB_2 phase	Space group P6/mmm: a = 3.020 Å, c = 3.050 Å	–	–
Theoretical ω – W_2B_5	Space group $P6_3/mmc$: a = 2.983 Å, c = 13.879 Å	–	–

The WB_{2-z} and $W_{0.76}Zr_{0.16}B_2$ coatings after 1h annealing in vacuum at the temperature of 650° did not delaminate and their roughness remained the same as before the annealing. Recorded XRD spectra of WB_{2-z} show a shift of the main XRD peak α - WB_2 (001) towards the higher 2θ angles. This phenomenon indicates a recovery of structural defects. It is known that annealing promotes the rearrangement of the atoms towards the places with lower energy, thus releasing the microstrains accumulated in the specimen. Similar behaviour of annealed WB_{2-z} coating is shown in ref. [**Błąd! Nie można odnaleźć źródła odwołania.**]. Another consequence of WB_{2-z} coating annealing is a significant reduction in ω – W_2B_5 (it drops from ~17% to 2%). In the case of the $W_{0.76}Zr_{0.16}B_2$ coating, the diffraction spectra did not change. Taking into account high boron deficiency, presented results indicates that (i) α phase field is

extended to lower boron contents, than ω phase and (ii) Zr stabilize α phase. Similar results were obtained for Ta doping [7].

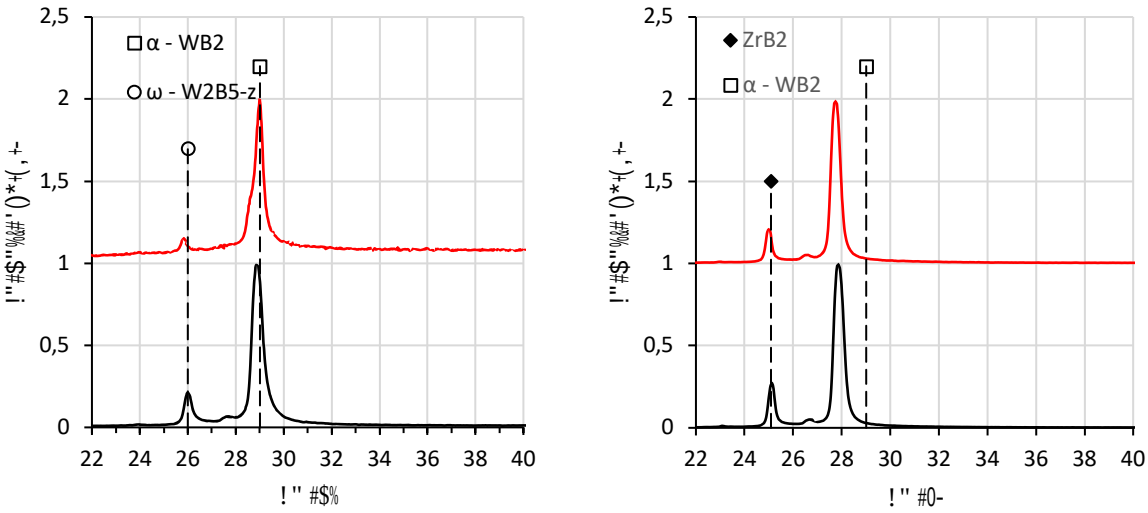

Fig. 10. XRD spectrum of WB_{2-z} (left) and $W_{0.76}Zr_{0.16}B_2$ (right) as deposited (black line) and after 1h vacuum annealing at 650°C (red line). Dotted line stands for theoretical standardized 2Θ-peak positions of ω – W_2B_5, α - WB_2 and ZrB2.

After annealing, the hardness of the WB_{2-z} coating increased from 45.8±0.6 to 48.3±3.4 GPa, and the Young modulus drop from 497±12 to 481±17 Gpa. However, reported result is within the accuracy range of the measurement. The pop-out effect is no longer observed in the unloading curve, see Fig. 11. This can be related to the reduction of internal strains and well thermally stabilized specimen. The mechanical properties of $W_{0.76}Zr_{0,16}B_2$ appear to be constant after annealing at 650°C.

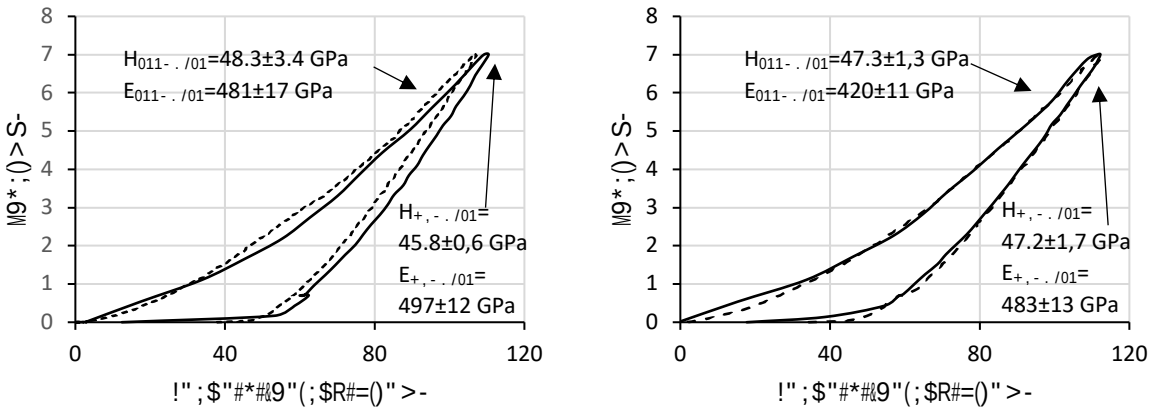

Fig. 11. Load-displacement curves of coatings as deposited (solid line) and after an hour vacuum annealing at 650°C (dashed line) a)WB_{2-z}, b) $W_{0.76}Zr_{0,16}B_2$. H_{AD_mean} – average hardness from 10 measurements of as deposited coating, H_{ann_mean} – average hardness from 10 measurements of the coating after an hour vacuum annealing at 650°C.

The influence of cyclic thermal loading on the properties of the deposited coatings seems to be more significant than the annealing process itself. First, the surface roughness increased to 35±7 and 21±5 nm for the WB_2 and $W_{0.76}Zr_{0.16}B_2$ coatings, respectively. A change in surface quality was also observed in the SEM images, where the appearance of a preferential grain growth can be observed. Moreover, in the case of WB_{2-z} coating, micro craters with a diameter of up to 2 µm were noticed, see Fig. 12.

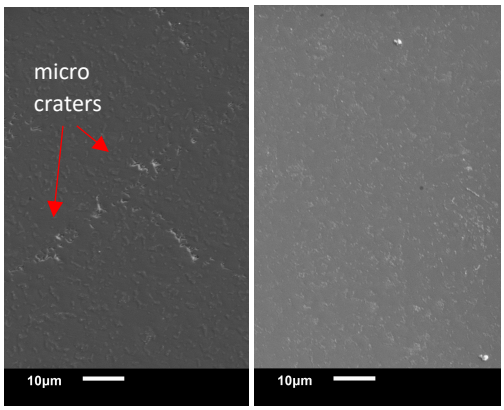

Fig. 12. SEM images of WB_2 (left) and $W_{0.76}Zr_{0.16}B_2$ after 50 thermal shocks (right).

The XRD spectra of WB_{2-z} coating after 50 thermal shocks show an increase in the ratio of ω-W_2B_5 to α-WB_2 phase and the presence of ω-W_2B_5 diffraction lines other than (004), see Fig. 13. It has been calculated that ω-W_2B_5 phase increases from 17 up to 27%. In the case of the $W_{0.76}Zr_{0.16}B_2$ coating, new diffraction lines originating from the ω-W_2B_5 phase were also observed. However the content of the above mentioned phase has not changed significantly. The XRD spectra of both tested coatings show a shift of the main diffraction lines towards smaller diffraction angles. This phenomenon indicates a uniform increase in strain which may result from the difference in thermal expansion coefficient between the substrate and the layer.

The different results reported after heating and thermal shocking may originate from the rate of change of the heat load. Fig. 2 shows the operation of the furnace, while the actual temperature changes on the surface of the layer will be much more abrupt (the thin layer will heat up and cool down rapidly). Due to the lower thermodynamic stability of the α phase, it is expected that this phase is reduced in the case of the WB_{2-z} coating. For the Zr-doped coatings, an alpha stabilization effect can be observed, which is in line with the simulations presented in Ref. [7].

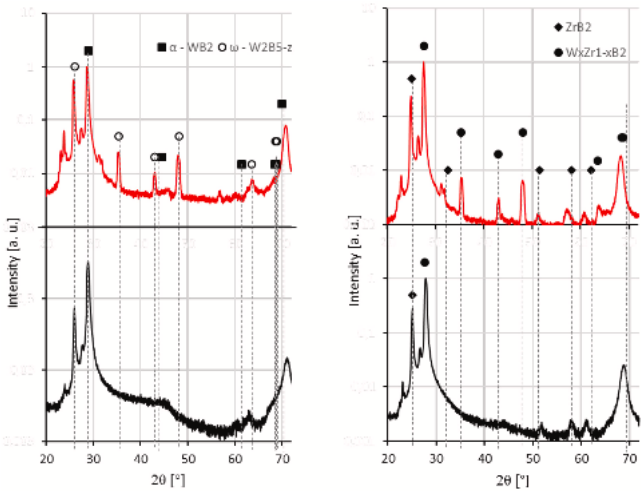

Fig. 13. XRD spectrum of WB_2 (left) and $W_{0.76}Zr_{0.16}B_2$ (right) as deposited (solid line) and after 50 shocks (dashed line).

The nanoindentation test shows that the heating-cooling cycles led to an increase in Young's modulus of about 50% for both WB_{2-z} and $W_{0.76}Zr_{0.16}B_2$ coatings (58 and 53%, respectively). The hardness increases by 28 and 17 %, respectively, for the WB_{2-z} and $W_{0.76}Zr_{0.16}B_2$ coatings. The increase in hardness and Young modulus may be due to residual stresses after thermal shocks. This subject will be further developed in the up-coming contribution of this group. Series of spherical nanoindentation tests with different indenter sizes are planned to be performed. This will allow us to calculate stress-strain curves

for these systems and ultimately will lead to calculation of different mechanical parameters like: shear stress, yield point, UTS or hardening exponent.

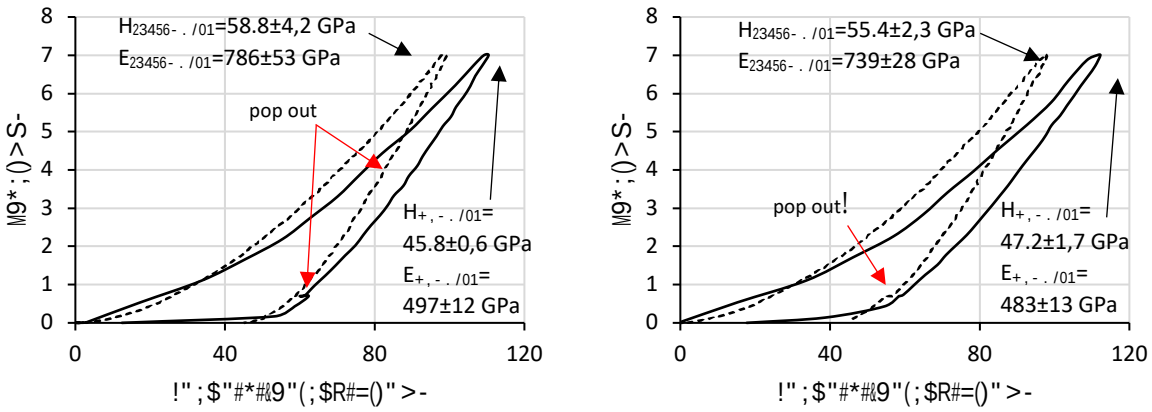

Fig. 14. Load-displacement curves of the coatings as deposited (solid line) and after 50 thermal shocks (dashed line) a)WB_{2-z}, b) $W_{0.76}Zr_{0,16}B_2$. H_{AD_mean} – average hardness from 10 measurements of as deposited coating, H_{shock_mean} – average hardness from 10 measurements of the coating after 50 shocks.

4. Conclusions

The experimentally obtained lattice parameters of WB_{2-z} coating are in good agreement (for α-WB_2 and ω-W_2B_5) with previously reported lattice parameter increase with increasing Zr content. Taking into account boron concentration, it can be stated that all deposited coatings have boron vacancies. According to the numerical simulations and available experimental data, one can summarize that α-phase is characterized by lower boron contents then ω phase. Moreover, Zr doping contributes formation of the compound having very negative formation energy and it stabilize α phase.

From the mechanical point of view, the deposited coatings are super hard showing hardness above a 44.5 GPa. W-Zr-B coatings have a hardness similar to WB_{2-z} and at the same time have a lower Young modulus. Thermal tests (annealing and cycling thermal loads) point to the conclusion that Zr doped coatings are characterized by better mechanical properties and have higher thermal stability. In addition to that, these coatings show to be less prone to cracking and have a lower Young's modulus.

Acknowledgement

This work was supported by the National Science Centre (NCN, Poland), Research Project: UMO-2017/25/B/ST8/01789. This work was co-financed by the National Centre for Research and Development (NCBR, Poland) under project no. TECHMATSTRATEGIII/ 0017/2019.

References

1. Y. M. Liu, C.L. Jiang, Z.L. Pei, H. Lei, J. Gong, C. Sun, Microstructure and properties of AlB2-type WB2 thin films deposited by direct-current magnetron sputtering, Surs. Coat. Technol. 245 (2014) 108–116
2. Yan!Ming Liu, Tong Li, Feng Liu, Zhi!Liang Pei, Thermal stability of WB2 and W-B-N deposited by magnetron sputtering, Acta Metallurgica Sinica 32 (2019) 136-144
3. J. Chrzanowska, Ł. Kurpaska, M. Giżyński, J. Hoffman, Z. Szymański, T. Mościcki, *Fabrication and characterization of superhard tungsten boride layers deposited by radio frequency magnetron sputtering*, Ceramics International 42 (10) (2016) 12221-12230

4. D. Garbiec, M. Wiśniewska, R. Psiuk, P. Denis, N. Levintant-Zayonts, V. Leshchynsky, R. Rubach, T. Mościcki, Zirconium alloyed tungsten borides synthetized by spark plasma sintering, Archives of civil and Mechanical Engineering 21 (37) (2021)
5. T. Mościcki, R. Psiuk, H. Słomińska, N. Levintant-Zayonts, D. Garbiec, M. Pisarek, P. Bazarnik, S. Nosewicz, J. Chrzanowska-Giżyńska, *Influence of overstoichiometric boron and titanium addition on the properties of RF magnetron sputtered tungsten borides, Surf. Coat. Technol. 390 (2020)* 125689-1-12
6. C. Fuger, B. Schwartz, T. Wojcik, V. Moraes, M. Weiss, A. Limbeck, A. Macauley, O. Hunold, P. Polcik, D. Primetzhofer, P. Felfer, P. H. Mayrhofer, H. Riedl, Influence of Ta on the oxidation resistance of WB2-z coatings, J. *Alloys Compounds 864 (2021) 158121*
7. V. Moraes, C. Fuger, V. Paneta, D. Primetzhofer, P. Polcik, H. Bolvardi, M. Arndt, H. Riedl, P. H. Mayrhofer, Substoichiometry and tantalum dependent thermal stability of α-structured W-Ta-B thin films, Scripta Materialia 155 (2018) 5-10
8. V. Moraes, H. Riedl, C. Fuger, P. Polcik, H. Bolvardi, D. Holec, P. H. Mayrhofer, Ab initio inspired design of ternary boride thin films, *Scientific Reports 8 (2018) 9288*
9. M. Mazdziarz, T. Moscicki, New zirconium diboride polymorphs – first principles calculations, Materials 13 (13) (2020) 3022-1-13.
10. Y.M.Liu,T.Li,F.Liu,Z.L.Pei,ThermalstabilityofWB2andW-B-Nfilmsdeposited by magnetron sputtering, Acta Metall. Sin. 32 (136) (2019) 136–144.
11. J. Berlin, Analysis of boron with energy dispersive x-ray spectrometry, Imaging Microsc. 13 (2011) 19–21.
12. J. Chen, S.J. Bull, On the factors affecting the critical indenter penetration for measurement of coating hardness, Vacuum 83 (2009) 911.
13. J. Chrzanowska-Giz˙yn´ska, P. Denis, S. Wo´zniacka, Ł. Kurpaska, Mechanical properties and thermal stability of tungsten boride films deposited by radio frequency magnetron sputtering, Ceram. Int. 44 (16) (2018) 19603–19611.
14. G. Greczynski, L. Hultman, C 1s peak of adventitious carbon aligns to the vacuum level: dire consequences for material's bonding assignment by photoelectron spectroscopy, ChemPhysChem 18 (2017) 1507–1512.
15. G. Greczynski, L. Hultman, Reliable determination of chemical state in x-ray photoelectron spectroscopy based on sample-work-function referencing to adventitious carbon: Resolving the myth of apparent constant binding energy of the C 1s peak, Appl. Surf. Sci. 451 (2018) 99–103.
16. O.V.Sobol,Influenceofdepositionconditionsandannealingtemperatureonphase composition and structure of W-B system ion-plasma condensates, Funct. Mater. 13 (3) (2006) 387–392
17. Powder Diffraction File 04–007-1000, International Center for Diffraction Data, 2011.
18. Powder Diffraction File 04–003-6624, International Center for Diffraction Data, 2011.
19. X.Y. Chen, X.Q. Chen, D.Z. Li, Y.Y. Li, Computational materials discovery: the case of the W-B system, Acts Cryst. C70 (2014) 81–103.
20. P. Scherrer, Go¨ttinger Nachrichten Gesell 2, 1918, p. 98.
21. B. Bor, D. Giuntini, B. Dom´enech, M.V. Swain, G.A. Schneider, Nanoindentation-based study of the mechanical behavior of bulk supercrystalline ceramic-organic nanocomposites, J. Eur. Ceram. Soc. 39 (2019) 3247–3256.

22. R. Hahn, V. Moraes, A. Limbeck, P. Polcik, P.H. Mayrhofer, H. Euchner, Electron-configuration stabilized (W, Al)B2 solid solutions, Acta Mater. 174 (2019)398–405.
23. H. Euchner, P.H. Mayrhofer, H. Riedl, F.F. Klimashin, A. Limbeck, P. Polcik, S. Kolozsvari, Solid solutionhardening of vacancy stabilized TixW1-xB2, Acta Mater. 101 (2015) 55–61.